SINGLE-SERIES SOLUTION TO THE RADIATION OF LOOP ANTENNA IN THE PRESENCE OF A CONDUCTING SPHERE

C. A. Valagiannopoulos

School of Electrical and Computer Engineering
National Technical University of Athens
GR 157–73. Zografou, Athens, Greece

Abstract—A ring source of arbitrary current backed by a perfectly conducting sphere is analyzed through Green's function formulation. The infinite double sum of the Green's function is written in terms of a single series by performing a transformation of the coordinate system. The resulting form is used for the numerical evaluation of the scattering integral. The operation of the coupled loop–sphere structure is understood via the discussion of several numerical results.

1. INTRODUCTION

The circular loop antenna is a popular radiator model studied through a variety of mathematical formulations and computational techniques. Electric currents on ring antennas have been extensively examined. In [1] analytical expressions of the near-zone integrals for a loop of arbitrary current are deduced with use of Lommel expansion. In [2] Pocklington's integral equation is formulated and method of moments is applied for the determination of the current on an arbitrarily large ring radiator in terms of step-pulse basis functions. Also in [3] exact series representations and far-zone approximations are given for the field of a loop with traveling-wave current distribution.

The radiation of loop antennas in the presence of other structures has also attracted much attention. In [4] two rings with different radii placed into a radially inhomogeneous cylinder are analyzed with use of cylindrical vector wave functions. Moreover, [5] provides a study of the effect of a multilayered chiral cartesian slab on the features of a ring antenna. A practical application of the model is given in [6] where the loop radiator is idealized as a magnetic dipole and its radiation between an anisotropic ionospheric plasma and the sea surface is investigated.

Finally, Felsen [7] presents a rigorous treatment for a structure with a ring source and an infinitively long cone which imitates the excitation of leaky-wave arrays.

Spherical structures are most commonly employed to modify the operation of the loop antenna. In [8] the magnetostatic theory is used for the determination of the image of a circular loop current in front of a permeable sphere. In [9] a complete analysis for a circular antenna inside a spherical biisotropic medium is provided. Also in [10] the method of moments is implemented to specify the current distribution of a circular loop in the presence of a layered chiral sphere. Even a spheroid scatterer is regarded in [11] where dyadic Green's functions are used for investigating the transmitted and reflected waves between the prolate multilayered spheroid and a radiating thin circular loop antenna.

In the present work a circular wire with arbitrary current radiates under the presence of a uniaxial perfectly conducting sphere. Spherical eigenfunctions, spherical harmonics and their attributes are used for the derivation of the azimuthal component of the dyadic Green's function. The double-series expression of this function is reduced to single-series form for the special case of a source posed on the axis of the spherical coordinate system. This property is expanded to have general validity regardless of the position of the source by a transformation of the coordinate system. Two successive rotations of the axes make the general term of the series more complicated but the double sum is converted into a single one.

The scattering integral is computed and the far-field formulas are obtained by using the single-series expression of the Green's function. After the validation of its formula we compared the time demanded for the evaluation of both expressions and in average the double-series is much more time consuming. To this end, a typical three-dimensional radiation pattern of the antenna is presented and a quite strong far-field power at the horizontal plane is observed. The variation of this power is shown with respect to the vertical loop-sphere distance. Many cases are examined corresponding to different operating frequencies, different loop radii and different physical dimensions of the sphere. Specific conclusions are drawn, some of them expected by physical intuition.

2. MATHEMATICAL FORMULATION

Suppose a spherical coordinate system with geometrical coordinates (r, θ, ϕ) and unitary vectors $(\hat{r}, \hat{\theta}, \hat{\phi})$. We use it to define an electromagnetic problem of suppressed harmonic time dependence

$e^{-i\omega t}$ inside vacuum area with wavenumber k_0. Each of the unitary vectors alters its direction for moving observation point and consequently the homogeneous vectorial Helmholtz equation (which is satisfied by the electromagnetic field) cannot be reduced to a scalar one. Therefore the three spherical eigenfunctions are employed for the field representation [12].

$$\mathbf{M}_{mn}(r,\theta,\phi) = \sqrt{n(n+1)}z_n(k_0 r)\mathbf{C}_{mn}(\theta,\phi) \tag{1}$$

$$\mathbf{N}_{mn}(r,\theta,\phi) = n(n+1)\frac{z_n(k_0 r)}{k_0 r}\mathbf{P}_{mn}(\theta,\phi)$$
$$+\sqrt{n(n+1)}\frac{z_n^d(k_0 r)}{k_0 r}\mathbf{B}_{mn}(\theta,\phi) \tag{2}$$

The third vectorial function $\mathbf{L}$ is indispensable only in the case of inhomogeneous materials and is excluded from the current consideration. The spherical harmonics $\mathbf{P},\mathbf{C},\mathbf{B}$ are defined as follows:

$$\mathbf{P}_{mn}(\theta,\phi) = \hat{r}e^{im\phi}P_{mn}(\theta) \tag{3}$$

$$\mathbf{C}_{mn}(\theta,\phi) = \frac{e^{im\phi}}{\sqrt{n(n+1)}}\left(\hat{\theta}\frac{im}{\sin\theta}P_{mn}(\theta) - \hat{\phi}P_{mn}^d(\theta)\right) \tag{4}$$

$$\mathbf{B}_{mn}(\theta,\phi) = \frac{e^{im\phi}}{\sqrt{n(n+1)}}\left(\hat{\theta}P_{mn}^d(\theta) + \hat{\phi}\frac{im}{\sin\theta}P_{mn}(\theta)\right) \tag{5}$$

where $P_{mn}(\theta)$ is the Legendre function of order m, degree n and argument $\cos\theta$. Its derivative with respect to θ is denoted as $P_{mn}^d(\theta)$. The function $z_n(k_0 r)$ can be either the spherical Bessel $j_n(k_0 r)$ (for regions including the origin) or the spherical Hankel of the first kind $h_n(k_0 r)$ (for regions including the infinite) [13]. The Riccati-Bessel function is defined as: $z_n^d(k_0 r) = \partial(k_0 r z_n(k_0 r))/\partial(k_0 r)$. In expressions (3)–(5) a change in the scalar arguments (θ,ϕ) affects the direction of the vectors $(\hat{r},\hat{\theta},\hat{\phi})$.

The spherical eigenfunctions are chosen suitably for easier application of the curl operator. Hence, the computations for the Faraday's or Ampere's law are carried out directly [14].

$$\nabla \times \mathbf{M}_{mn}(r,\theta,\phi) = k_0 \mathbf{N}_{mn}(r,\theta,\phi) \tag{6}$$
$$\nabla \times \mathbf{N}_{mn}(r,\theta,\phi) = k_0 \mathbf{M}_{mn}(r,\theta,\phi) \tag{7}$$

As far as the spherical harmonics are concerned, they exhibit certain orthogonality properties:

$$\int_0^{2\pi}\int_0^{\pi}\mathbf{C}_{mn}(\theta,\phi)\cdot\mathbf{C}_{\mu\nu}(\theta,\phi)\sin\theta d\theta d\phi = \frac{4\pi}{2n+1}(-1)^m\delta_{m(-\mu)}\delta_{n\nu} \tag{8}$$

$$\int_0^{2\pi}\int_0^{\pi}\mathbf{B}_{mn}(\theta,\phi)\cdot\mathbf{B}_{\mu\nu}(\theta,\phi)\sin\theta d\theta d\phi\ =\ \frac{4\pi}{2n+1}(-1)^m\delta_{m(-\mu)}\delta_{n\nu}\ \ (9)$$

$$\int_0^{2\pi}\int_0^{\pi}\mathbf{C}_{mn}(\theta,\phi)\cdot\mathbf{B}_{\mu\nu}(\theta,\phi)\sin\theta d\theta d\phi\ =\ 0 \qquad\qquad (10)$$

where δ_{mn} is the Kronecker's delta. By inspection of (3)–(5), one can extract the following relations, useful when applying boundary conditions on spherical surfaces:

$$\hat{r}\times\mathbf{P}_{mn}(\theta,\phi)\ =\ \mathbf{0} \qquad\qquad (11)$$

$$\hat{r}\times\mathbf{C}_{mn}(\theta,\phi)\ =\ \mathbf{B}_{mn}(\theta,\phi) \qquad\qquad (12)$$

$$\hat{r}\times\mathbf{B}_{mn}(\theta,\phi)\ =\ -\mathbf{C}_{mn}(\theta,\phi) \qquad\qquad (13)$$

The orthogonality equations (8)–(10) are valid only for integer indices, that is why we use the symbol δ_{mn}. The parameter m is integer only when the considered structure is azimuthally entire because a 2π periodicity for the ϕ-dependent quantities is demanded. In the same way when the configuration is θ-entire the parameter n is integer, otherwise the Legendre functions are singular at $\theta = 0, \pi$. We are interested in both ϕ — and θ — entire constructions. By taking into account that $P_{mn}(\theta) = P_{mn}^d(\theta) = 0$ for $|m| > n$ and by exploiting the opposite-order relations of Bessel functions, the value intervals of integers m, n are restricted. In particular, the linearly independent terms of the double sums with respect to m, n are only those with $m \in [-n, n]$ and $n \in [1, +\infty)$. Even though the sum with respect to m is not infinite, the difficulties of computing a double series for each field quantity remain.

The preceding formulas are necessary for the analysis of the investigated device. Consider a perfectly conducting (PEC) sphere of radius a the center of which coincides with the origin of the spherical coordinate system. Cartesian (x, y, z) coordinates can be used alternatively. A thin circular wire, parallel to the horizontal $x-y$ plane, is located across the edge $\{r = R_0, \theta = \Theta_0\}$ with an external radius of $R_0 > a$ and $\Theta_0 \in (0, \pi)$. The radius of the loop equals $b = R_0 \sin\Theta_0$ and $I(\phi)$ (in Amperes) stands for the arbitrary azimuthal function of the line current flowing the wire. The whole structure is appeared in Fig. 1 and placed inside vacuum area (k_0, ζ_0). Our purpose is to find a computationally effective method to evaluate the influence of the spherical scatterer on the radiation of the loop antenna.

3. DOUBLE-SERIES GREEN'S FUNCTION

Successful treatment of the aforementioned problem requires the explicit form of the electric-type dyadic Green's function of the
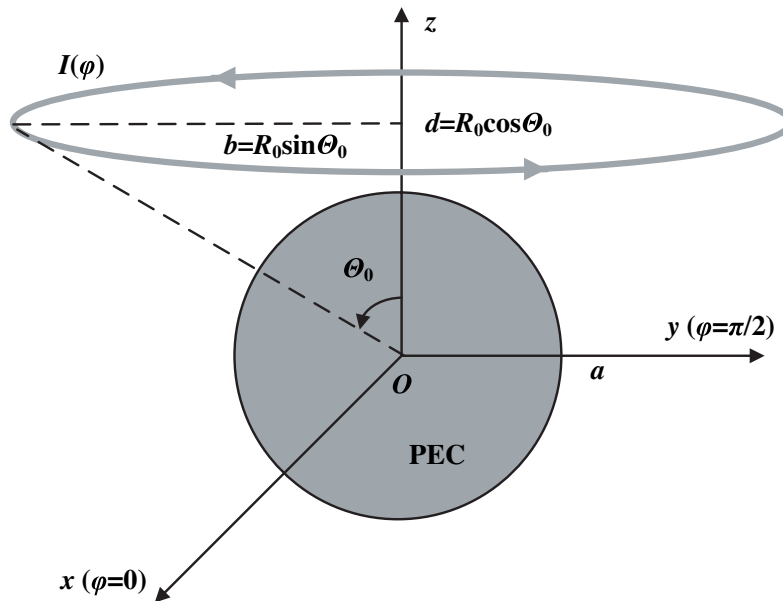
Figure 1. The physical configuration of the device. A circular loop antenna with arbitrary electric current $I(\phi)$ and radius $b = R_0 \sin \Theta_0$ is placed at distance $d = R_0 \cos \Theta_0$ above the center of a sphere with radius a. The sphere is perfectly conducting (PEC) and scatters the field produced by the antenna.

PEC sphere [15]. This is a matrix that contains the electric field vectors developed by an infinitesimal electric dipole for all possible polarizations in the presence of the sphere. The quantities refer to an observation point (r, θ, ϕ), while the source is located on the point (R, Θ, Φ) and has a specific magnitude [15]. As we are interested for points far from the radiation device, we suppose $r > R$. The imposed excitation is azimuthal (loop current) and therefore only the ϕ component of the dyadic Green's function is necessary for the determination of the scattered field. For this reason the electric field of a ϕ-polarized dipole is the only prerequisite to proceed farther.

This vectorial function is denoted by $\mathbf{G}(r, \theta, \phi)$ (the variables R, Θ and Φ are implicit) and can be readily derived. One can describe the electric field as weighted double sums of the spherical eigenfunctions (1),(2) and deduce the magnetic field via (6),(7). By imposing continuity of the tangential electric and singular discontinuity (due to the point source) of the tangential magnetic field at $r = R$,

the first two boundary conditions are derived. The third one emanates from the demand for vanishing tangential electric field on the spherical scatterer at $r = a$ and use of (11)–(13). The arbitrary coefficients of the sums are specified by projecting the three boundary conditions on the sets of the spherical harmonics and exploiting the orthogonality properties (8)–(10). The desired Green's function for the outer region $r > R$ is given by

$$
\mathbf{G}(r,\theta,\phi) = \sum_{n=1}^{+\infty} \sum_{m=-n}^{n} \Bigg[(U_0(m,n) + U_1(m,n)) n(n+1) \frac{h_n(k_0 r)}{k_0 r} \mathbf{P}_{mn}(\theta,\phi)
$$
$$
+ (V_0(m,n) + V_1(m,n)) \sqrt{n(n+1)} h_n(k_0 r) \mathbf{C}_{mn}(\theta,\phi)
$$
$$
+ (U_0(m,n) + U_1(m,n)) \sqrt{n(n+1)} \frac{h_n^d(k_0 r)}{k_0 r} \mathbf{B}_{mn}(\theta,\phi) \Bigg] \quad (14)
$$

where the weighting coefficients are defined by the following expressions:

$$
U_0(m,n) = m \frac{2n+1}{n(n+1)} \frac{(n-m)!}{(n+m)!} \frac{j_n^d(k_0 R)}{4\pi R} \frac{P_{mn}(\Theta)}{\sin \Theta} e^{-im\Phi} \quad (15)
$$

$$
U_1(m,n) = -m \frac{j_n^d(k_0 a)}{h_n^d(k_0 a)} \frac{2n+1}{n(n+1)} \frac{(n-m)!}{(n+m)!} \frac{h_n^d(k_0 R)}{4\pi R} \frac{P_{mn}(\Theta)}{\sin \Theta} e^{-im\Phi} \quad (16)
$$

$$
V_0(m,n) = -i \frac{2n+1}{n(n+1)} \frac{(n-m)!}{(n+m)!} \frac{k_0 j_n(k_0 R)}{4\pi} P_{mn}^d(\Theta) e^{-im\Phi} \quad (17)
$$

$$
V_1(m,n) = i \frac{j_n(k_0 a)}{h_n(k_0 a)} \frac{2n+1}{n(n+1)} \frac{(n-m)!}{(n+m)!} \frac{k_0 h_n(k_0 R)}{4\pi} P_{mn}^d(\Theta) e^{-im\Phi} \quad (18)
$$

The Green's function in geometric units has dimensions of inverse length.

4. SINGLE-SERIES GREEN'S FUNCTION

The derived quantity (14) can be used straightforwardly for the computation of the total electric field in the far region of the antenna. It would be preferable though to supply an alternative derivation of the Green's function to avoid the cumbersome double series calculation. In this analysis the observation point will be notated with primes (r', θ', ϕ'), corresponding to a duplicated spherical coordinate system, just for the sake of generality. If one evaluates the formulas (14)–(18) for $\Theta \to 0^+$ (at the primed observation point), only two terms of the

summation with respect to m will be nonzero ($m = \pm 1$). In other words, due to the following property of the Legendre functions

$$\lim_{\Theta \to 0^+} \frac{P_{mn}(\Theta)}{\sin \Theta} = \lim_{\Theta \to 0^+} P_{mn}^d(\Theta) = \begin{cases} 1/2 & , m = -1 \\ -n(n+1)/2 & , m = 1 \\ 0, & , m \neq \pm 1 \end{cases} \quad (19)$$

the electric field of a dipole posed on the axial direction $\Theta = 0$ (or the antipodal one $\Theta = \pi$) is given by a single series (the second sum contains only two terms). We also suppose $\Phi = 0$ to regard a ϕ'-polarized (or alternatively y'-polarized) dipole source posed at height R on the z' axis of the primed coordinate system. Its field is given by the following simplified function $\mathbf{G}'$:

$$\begin{aligned} \mathbf{G}'(r', \theta', \phi') = \sum_{n=1}^{+\infty} \Bigg[& (U_0^+(n) + U_1^+(n))n(n+1)\frac{h_n(k_0 r')}{k_0 r'}\mathbf{P}_{1n}(\theta', \phi') \\ & + (V_0^+(n) + V_1^+(n))\sqrt{n(n+1)}h_n(k_0 r')\mathbf{C}_{1n}(\theta', \phi') \\ & + (U_0^+(n) + U_1^+(n))\sqrt{n(n+1)}\frac{h_n^d(k_0 r')}{k_0 r'}\mathbf{B}_{1n}(\theta', \phi') \\ & + U_0^-(n) + U_1^-(n))n(n+1)\frac{h_n(k_0 r')}{k_0 r'}\mathbf{P}_{(-1)n}(\theta', \phi') \\ & + (V_0^-(n) + V_1^-(n))\sqrt{n(n+1)}h_n(k_0 r')\mathbf{C}_{(-1)n}(\theta', \phi') \\ & + (U_0^-(n) + U_1^-(n))\sqrt{n(n+1)}\frac{h_n^d(k_0 r')}{k_0 r'}\mathbf{B}_{(-1)n}(\theta', \phi') \Bigg] \end{aligned}$$

$$(20)$$

The complex coefficients are determined by the pairs of equations below:

$$U_0^-(n) = -(2n+1)\frac{j_n^d(k_0 R)}{8\pi R} \qquad\qquad U_0^+(n) = \frac{U_0^-(n)}{n(n+1)} \qquad (21)$$

$$U_1^-(n) = (2n+1)\frac{h_n^d(k_0 R)}{8\pi R}\frac{j_n^d(k_0 a)}{h_n^d(k_0 a)} \qquad U_1^+(n) = \frac{U_1^-(n)}{n(n+1)} \qquad (22)$$

$$V_0^-(n) = -i(2n+1)\frac{k_0 j_n(k_0 R)}{8\pi} \qquad V_0^+(n) = -\frac{V_0^-(n)}{n(n+1)} \qquad (23)$$

$$V_1^-(n) = i(2n+1)\frac{k_0 h_n(k_0 R)}{8\pi}\frac{j_n(k_0 a)}{h_n(k_0 a)} \quad V_1^+(n) = -\frac{V_1^-(n)}{n(n+1)} \qquad (24)$$

5. COORDINATE TRANSFORMATION

Hitherto, the two coordinate systems (unprimed and primed) were not correlated while primed one was considered as arbitrary. Now, we define the primed spherical coordinate system as that with respect to which the electric field of the ϕ-polarized dipole source at (R, Θ, Φ) is given by (20). To put it another way, the ϕ'-polarized source at $(R, 0, 0)$ produces the field of (14). This procedure is aiming at expressing (14) as a single series by finding the transformation relations between the primed system's parameters (geometrical coordinates and unitary vectors) and the unprimed ones. To specify the primed coordinate system, rotate the unprimed with respect to z axis by angle Φ and the resulting one (call it double primed) with respect to its own y'' axis by angle Θ. To this end, the transformation formula connecting the two sets of cartesian parameters is found instantly [16].

$$
\begin{bmatrix} x' & \hat{x}' \\ y' & \hat{y}' \\ z' & \hat{z}' \end{bmatrix} = \begin{bmatrix} \cos\Theta & 0 & -\sin\Theta \\ 0 & 1 & 0 \\ \sin\Theta & 0 & \cos\Theta \end{bmatrix} \cdot \begin{bmatrix} \cos\Phi & \sin\Phi & 0 \\ -\sin\Phi & \cos\Phi & 0 \\ 0 & 0 & 1 \end{bmatrix} \cdot \begin{bmatrix} x & \hat{x} \\ y & \hat{y} \\ z & \hat{z} \end{bmatrix}
\tag{25}
$$

The expressions converting the spherical unitary vectors to cartesian and vice-versa are well-known.

$$
\begin{bmatrix} \hat{x} \\ \hat{y} \\ \hat{z} \end{bmatrix} = \begin{bmatrix} \sin\theta\cos\phi & \cos\theta\cos\phi & -\sin\phi \\ \sin\theta\sin\phi & \cos\theta\sin\phi & \cos\phi \\ \cos\theta & -\sin\theta & 0 \end{bmatrix} \cdot \begin{bmatrix} \hat{r} \\ \hat{\theta} \\ \hat{\phi} \end{bmatrix}
\tag{26}
$$

$$
\begin{bmatrix} \hat{r}' \\ \hat{\theta}' \\ \hat{\phi}' \end{bmatrix} = \begin{bmatrix} \sin\theta'\cos\phi' & \sin\theta'\sin\phi' & \cos\theta' \\ \cos\theta'\cos\phi' & \cos\theta'\sin\phi' & -\sin\theta' \\ -\sin\phi' & \cos\phi' & 0 \end{bmatrix} \cdot \begin{bmatrix} \hat{x}' \\ \hat{y}' \\ \hat{z}' \end{bmatrix}
\tag{27}
$$

To evaluate (27), one should also know the relations defining the spherical coordinates as functions of the cartesian ones.

$$
r' = \sqrt{x'^2 + y'^2 + z'^2} = r \qquad \theta' = \arccos\frac{z'}{r'} \qquad \phi' = \arctan\frac{y'}{x'}
\tag{28}
$$

It is noticeable that due to the nature of transformation (two successive spherical rotations with no translation), both the radial coordinate $(r' = r)$ and the corresponding unitary vector $(\hat{r}' = \hat{r})$ are left unaltered. The inverse relations of (28) are also needed to express the Green's function in spherical coordinates:

$$
x = r\cos\phi\sin\theta \qquad\qquad y = r\sin\theta\sin\phi \qquad\qquad z = r\cos\theta \tag{29}
$$

By substituting (25)–(29) to (20) the single-series expression of the requested Green's function **G** is deduced.

6. SCATTERING INTEGRAL

If the single-series formula of $\mathbf{G}(r, \theta, \phi)$ is evaluated at $(R = R_0, \Theta = \Theta_0)$, the final Green's function required for the computation of the total electric field is obtained. It is denoted as $\mathbf{g}(r, \theta, \phi, \Phi)$ with an extra azimuthal argument Φ which is the dummy integration variable. The electric field is given by the following scattering integral [15]:

$$\mathbf{E}(r, \theta, \phi) = ik_0\zeta_0 R_0 \sin\Theta_0 \int_0^{2\pi} \mathbf{g}(r, \theta, \phi, \Phi)I(\Phi)d\Phi \qquad (30)$$

Because of the complicated dependence of the function $\mathbf{g}$ on the variable Φ (due to the successive transformation relations), an analytic integration in (30) is not possible. For this reason numerical integration is carried out instead by implementing the trapezoidal rule for F equispaced points within the interval $\Phi \in (0, 2\pi)$. Through this approach the arbitrary function of the current $I(\Phi)$ is integrated straightforwardly with no need of prior expansion to Fourier series [9]. The basic disadvantage of the proposed method is the computational cost owed to the numerical integration but such a procedure meets no difficulty. The integration interval is finite, the integrands are smooth and without rapid oscillations (for common current distributions $I(\Phi)$).

To investigate the far-field quantities of the loop antenna under the presence of the spherical scatterer, asymptotic evaluation of the developed field for $k_0 r \to +\infty$ is required. As the approximation concerns the radial coordinate which is not affected by the transformation, the dependencies on $r = r'$ will be similar to these in (20). Hence, the following asymptotic expressions can be used:

$$ih_n(k_0 r), h_n^d(k_0 r) \sim (-i)^{n-1}\frac{e^{ik_0 r}}{k_0 r}e^{-i\frac{\pi}{4}} \quad , k_0 r \to +\infty \qquad (31)$$

Thereby the radiated power of the antenna is computed via the following well-known formula:

$$S(\theta, \phi) = \frac{r^2}{2\zeta_0} \lim_{r \to +\infty} \left[|E_\theta(r, \theta, \phi)|^2 + |E_\phi(r, \theta, \phi)|^2\right] \qquad (32)$$

7. NUMERICAL RESULTS

A set of computer programs has been developed for the calculation of the far-field patterns of the coupled loop-sphere structure through the single-series formula obtained from (20). In all the following examples the infinite sums with respect to n are truncated by keeping

N terms and the numerical integrations are executed by evaluating the integrands at F equispaced points. Both parameters are chosen large enough to achieve convergence for the investigated quantities. As far as the number of trapezoidal integration points is concerned, a choice of $F = 40$ is adequate for all the examined models.

Before presenting the results, it is essential to validate the single-series formula and check if its values coincide with those of double-series expression. In Fig. 2 the real part of the azimuthal electric field is represented as function of the normalized radial distance r to the radius R_0 for three different polar angles $\theta = \pi/4, \pi/3, \pi/2$. The field exhibits a slowly dumping behavior as the observation point gets distant from the source. The curves are produced with (20) and the discrete points with (14). In this example the operating frequency equals $f = 1200\,\text{MHz}$ and we suppose a line current located at $\Theta_0 = \pi/2$ which is constant $I(\Phi) = 1\,\text{A}$ (that is why the azimuthal angle ϕ of the observation point is not mentioned). The radius
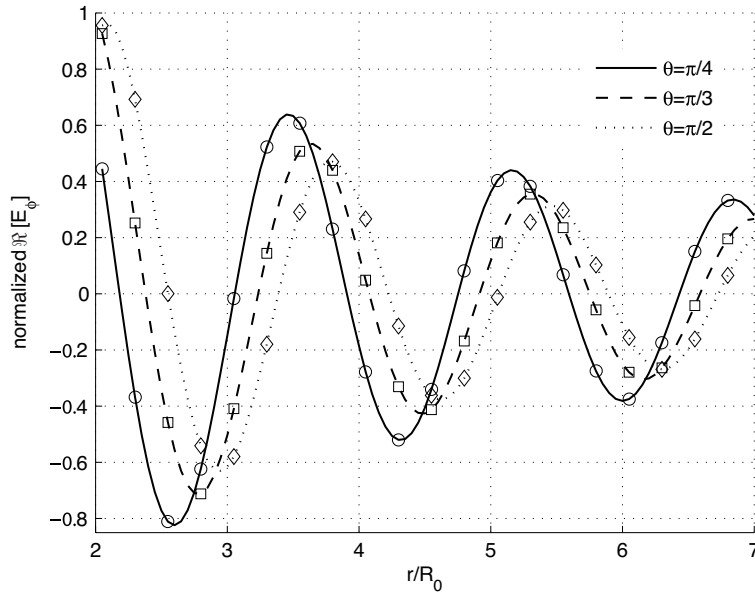

Figure 2. Variation of the real part of the dominant ϕ component of the total electric field as function of the normalized radial distance for three different polar angles of observation point. The curves correspond to the single-series formula and the discrete points to the double-series one. Plot parameters: $R_0 = 15\,\text{cm}$, $a = 10\,\text{cm}$, $\Theta_0 = \pi/2$, $f = 1200\,\text{MHz}$, $I(\Phi) = 1\,\text{A}$.

of the PEC sphere equals to $a = 10$ cm and the external one's to $R_0 = 15$ cm. Each measurement series is normalized by its sample with maximum magnitude. Only the azimuthal electric component is depicted because it is dominant, a property imposed by the nature of the excitation. As it is expected, the results from both formulas are identical. Similar checks are performed for both parts (real and imaginary) of all the components, for a variety of input parameters with the same coincidence.

After validating the single-series expression, it would be interesting to show how faster the evaluation gets due to its reduced computational complexity. In Fig. 3 the time gain of using (20) instead of (14) is presented as function of the truncation upper limit N for a specific observation point ($r = 20$ cm, $\theta = \pi/4$, $\phi = \pi/6$) and a constant source point ($R = 10$ cm, $\Theta = 4\pi/5$, $\Phi = 2\pi/3$). The calculations were carried out on an ATHLON 2 GHz processor and the results are expressed in db because of the large magnitudes. The time gain is increasing with N and usually exceeds 50 db (more than 300 times faster). One could point out that if (14) demands a smaller
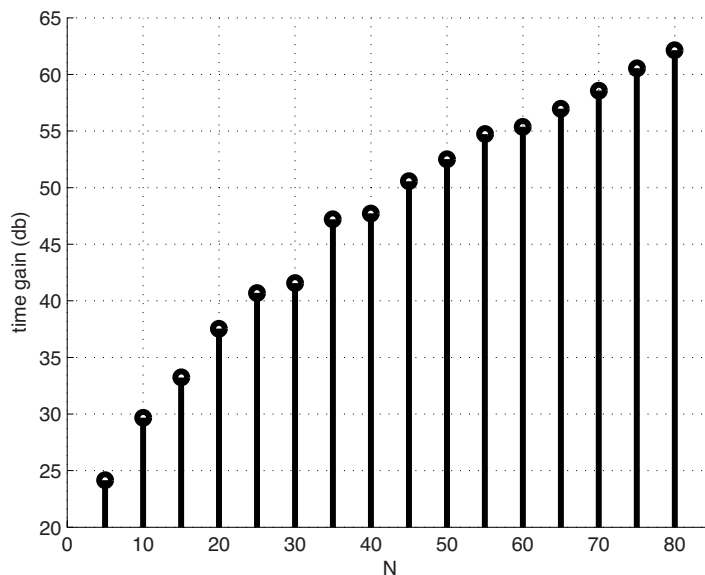

Figure 3. Time gain in db of using the single-series formula instead the double-series formula as function of the number of terms N. Plot parameters: $r = 20$ cm, $\theta = \pi/4$, $\phi = \pi/6$, $R = 10$ cm, $a = 0.7R_0$, $\Theta = 4\pi/5$, $\Phi = 2\pi/3$, $f = 1600$ MHz.

truncation limit for convergence than (20) does, the comparison shown in Fig. 3 is unfair. This is not the case as the transformation of the coordinates does not affect the radial dependencies and therefore the adequate N for convergence is the same for both formulas. As a rule of thumb $N = 120$ terms per wavelength of R_0 is sufficient for all the following examples.

A three-dimensional radiation pattern of the loop-sphere antenna is presented in Fig. 4 for a nonuniform current distribution $I(\Phi) = 1 + \cos 2\Phi$ A located at $\Theta_0 = \pi/6$. The radii of the structure are chosen equal to $a = 10$ cm and $R_0 = 15$ cm combined with an operating frequency of $f = 1000$ MHz. It is noticeable that the radiation power follows the ϕ dependency of the excitation current. The far-field is more powerful for $\theta < \pi/2$ where two local maxima are exhibited, contrary to the half plane $\theta > \pi/2$ where the scatterer shadows the region. The main lobes close to the angle $\theta = \pi/2$ are flattened and the radiation intensity is greater there. This property is general for the range of device parameters we regard: at $\theta = \pi/2$ local maxima (which are global sometimes) are recorded. Even though the radiator possesses an asymmetric pattern with respect to x-y horizontal plane, the radiation along this surface is an interesting process to be investigated. Despite the fact that significant portions of power
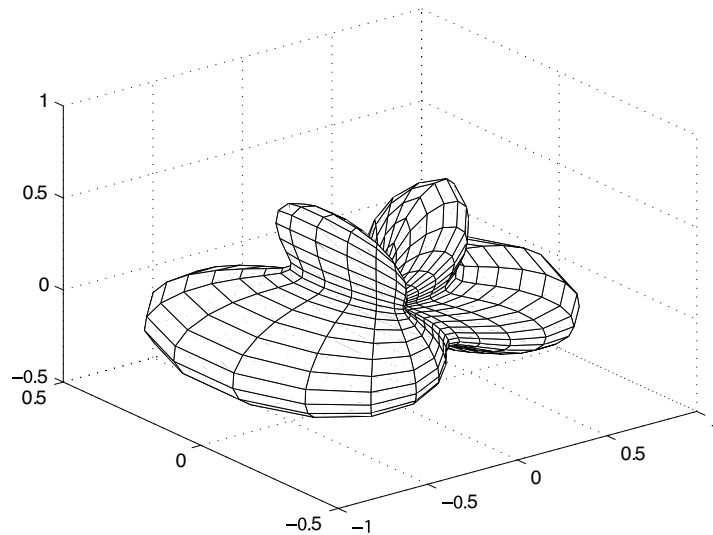

Figure 4. Three-dimensional normalized radiation pattern of the loop antenna backed by a conducting spherical reflector. Plot parameters: $R_0 = 15$ cm, $a = 10$ cm, $\Theta_0 = \pi/6$, $f = 1000$ MHz, $I(\Phi) = 1 + \cos 2\Phi$ A.

are channeled to other directions, the power propagation for the rays $\theta = \pi/2$ (which do not essentially correspond to main lobes) is worth to be examined.

In Fig. 5a constant current $I(\Phi) = 1\,\mathrm{A}$ is supposed (azimuthal independence) and the radiated power at $\theta = \pi/2$ is presented as function of the ratio d/a for $a = 6\,\mathrm{cm}$ and $b/a = 1.1$. Four operating frequencies are considered $f = 400, 800, 1200, 1600\,\mathrm{MHz}$ and only positive values of d are regarded due to symmetry with respect to the observation plane. As it is expected, the fluctuation of the far-field power with varying d/a becomes greater with increasing frequency. Furthermore, within the considered spatial range, the peak power achieved in each case is proportional to the oscillating frequency. Specifically for the lower one ($f = 400\,\mathrm{MHz}$), the response of the system is almost negligible. One could also notice that for $d/a \to 0$ the power is diminishing for all the operating frequencies. That leads us to the conclusion that the spherical scatterer disturbs the operation of the antenna when its center coincides with the center of the loop.

In Fig. 5b the same quantities are depicted as functions of the same parameters but with a sphere two times larger: $a = 12\,\mathrm{cm}$. The curves for $f = 400, 800\,\mathrm{MHz}$ of Fig. 5b are identical to those of Fig. 5a for $f = 800, 1600\,\mathrm{MHz}$. That is natural because the electrical dimensions of the device are the same in the corresponding cases. The increasing relation between the maximum radiated power and the frequency indicated by Fig. 5a is not valid for the wider spatial window shown in Fig. 5b. The magnitude of the far-field oscillations for $f = 800, 1200, 1600\,\mathrm{MHz}$ is almost the same and only the frequencies of the oscillations change.

In Fig. 6a we regard a small sphere of $a = 6\,\mathrm{cm}$ with $f = 1000\,\mathrm{MHz}$. Again the radiated power at $\theta = \pi/2$ is observed with respect to d/a for six different normalized radii of the loop: $b/a = 0.3, 0.6, 0.9, 1.2, 1.5, 1.8$. The current is again constant $I(\Phi) = 1\,\mathrm{A}$. For the cases with $b < a$, only the configurations of $d > a$ are examined, something imposed by the physical dimensions. It is obvious that when the ring has smaller radius than the sphere and is located too close to the spherical surface, the antenna operation fails. Opposite images are developed in the internal of the scatterer neutralizing the excitation. Moreover, the response of the radiator is more significant for larger loops. It is natural because longer wires of constant current produces more powerful fields. Finally, the blocking effect of the sphere for $d = 0$ is attenuated for increasing b/a because the physical radius of the sphere is reduced compared to the largest dimension of the device.

A similar set of curves for a larger sphere with $a = 12\,\mathrm{cm}$ is depicted in Fig. 6b. In the cases of $b < a$ sharper maxima for greater
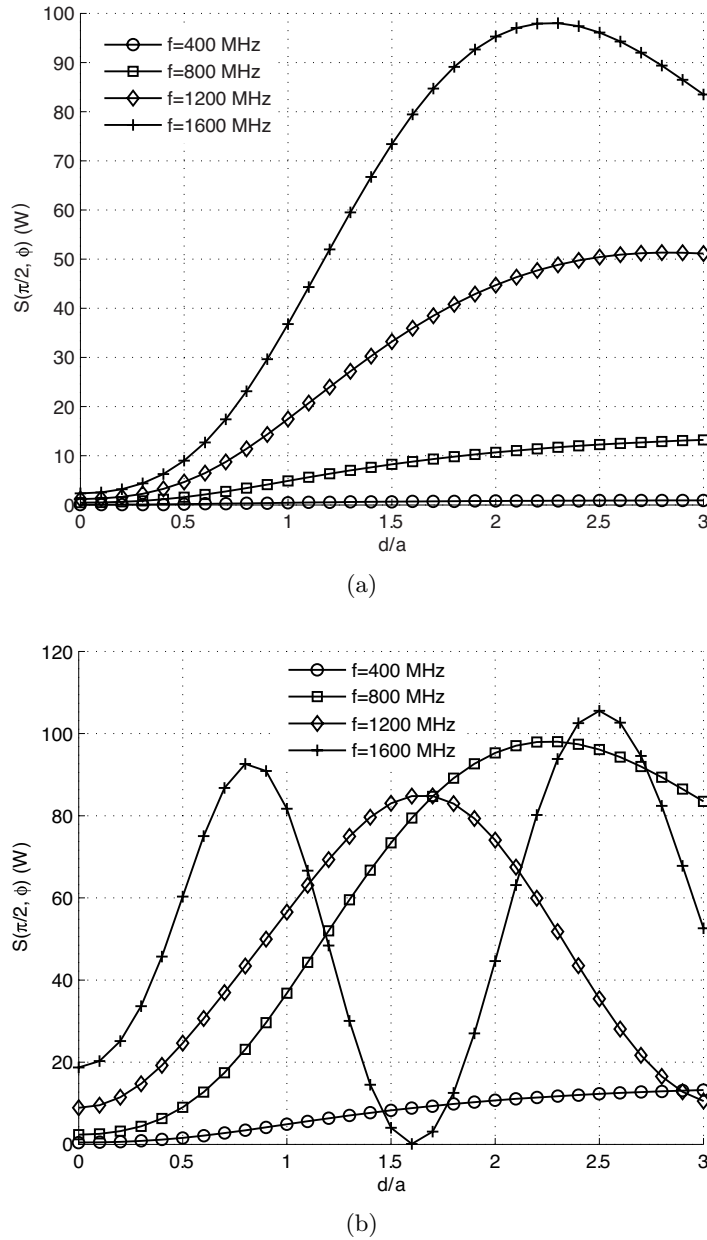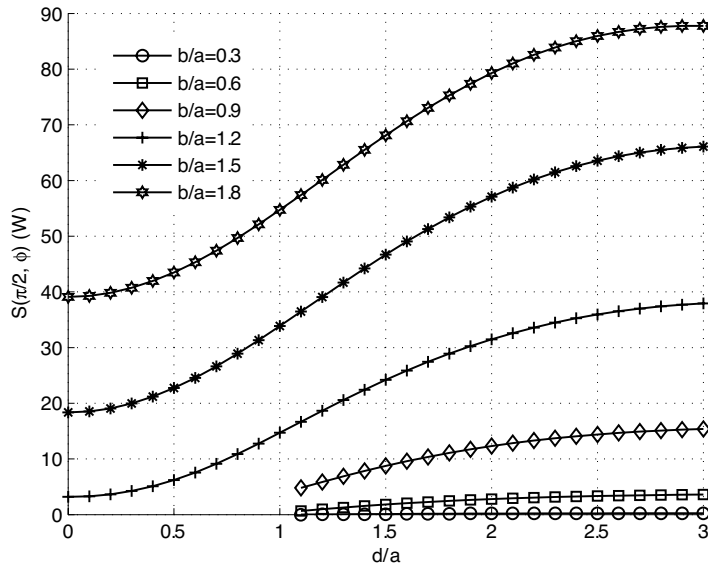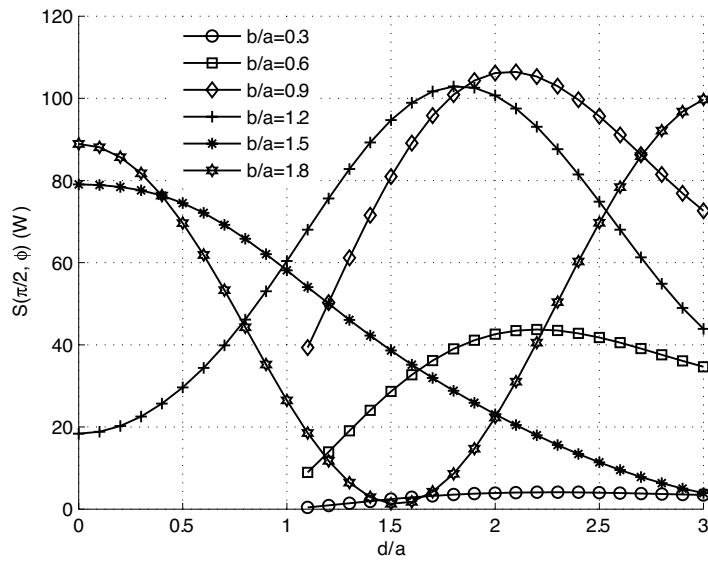
(a)

(b)

Figure 5. Radiation power (in Watts) at the direction $\theta = \pi/2$ as function of the vertical position of the ring for four different operating frequencies. Plot parameters: $b/a = 1.1$, $I(\Phi) = 1\,\text{A}$. The radius of the sphere equals to: (a) $a = 6\,\text{cm}$ (b) $a = 12\,\text{cm}$.

(a)

(b)

Figure 6. Radiation power (in Watts) at the direction $\theta = \pi/2$ as function of the vertical position of the ring for six different radii of the loop. Plot parameters: $f = 1000\,\text{MHz}$, $I(\Phi) = 1\,\text{A}$. The radius of the sphere equals to: (a) $a = 6\,\text{cm}$ (b) $a = 12\,\text{cm}$.

current loops are noticed, reflecting the impact of the source. Also the curves corresponding to $b/a = 1.2, 1.8$ have an reverse dependency on d/a: when the first is increasing the other is decreasing and vice-versa. It is thus sensible to suppose that there is a specific ratio $1.2 < b/a < 1.8$ (in the particular model) for which zero variation of the radiation power with respect to d/a is achieved (as if the sphere was absent). Indeed, the fluctuation of the investigated quantity is much lesser for $b/a = 1.5$.

8. CONCLUSIONS

The effect of a perfectly conducting spherical scatterer on the features of a circular loop antenna with arbitrary current is analyzed. Because of the nature of the excitation, only the azimuthal component of the dyadic Green's function is required which is given in a double-series expression. Through a transformation of the spherical coordinate system consisting of two successive rotations, the double sum of the solution is converted to a single sum. The last expression is less time consuming than the first one. With use of this effective formula the radiated power along the horizontal plane is observed. The variation of this quantity with respect to the relative loop-sphere position is presented. Various operating frequencies, numerous loop's radii and different sphere's sizes are considered. Some conclusions concerning the operation of the coupled structure are inferred such as the blocking effect of the sphere when is located at the center of the loop.

The transformation of the coordinate system simplifying the expression of the azimuthal Green's function can be utilized for all the other components. In this way the proposed method is useful to obtain the dyadic Green's function of a conducting sphere in single-series form. As far as the characteristics of the antenna are concerned, similar techniques can be utilized for understanding the influence of permeable multilayered spheres or cylinders on the operation of loop radiators.

REFERENCES

1. Werner, D. H., "An exact integration procedure for vector potential of thin circular loop antennas," *IEEE Trans. Antennas Propag.*, Vol. 44, No. 2, 157–165, 1996.
2. Anastassiu, H. T., "Fast, simple and accurate computation of the currents on an arbitrarily large circular loop antenna," *IEEE Trans. Antennas Propag.*, Vol. 54, No. 3, 860–866, 2006.

3. Werner, D. H., "Near-field and far-field expansions for traveling-wave circular loop antennas," *Progress In Electromagnetics Research*, PIER 28, 29–42, 2000.

4. Yin, W. Y., G. H. Nan, and I. Wolff, "Electromagnetic fields of two thin circular loop antennas in a radially multilayered biisotropic cylinder," *Progress In Electromagnetics Research*, PIER 21, 247–272, 1999.

5. Yin, W. Y., L. W. Li, T. S. Yeo, and M. S. Leong, "Electromagnetic fields of a thin circular loop antenna above a (un)grounded multilayered chiral slabs," *Progress In Electromagnetics Research*, PIER 30, 131–156, 2001.

6. Li, K., H. Q. Zhang, and W. Y. Pan, "The VLF field on the sea surface generated by the space borne loop antenna," *Journal of Electromagnetic Waves and Applications*, Vol. 18, No. 1, 121–135, 2004.

7. Felsen, L. B., "Radiation from ring sources in the presence of a semi–infinite cone," *IRE Trans. Antennas Propag.*, Vol. 7, No. 4, 168–180, 1959.

8. Lindell, I. V., E. A. Lehtola, and K. I. Nikoskinen, "Magnetostatic image theory for an arbitrary current loop in front of a permeable sphere," *IEEE Trans. Magnetics*, Vol. 29, No. 5, 2202–2206, 1993.

9. Yin, W. Y., G. H. Nan, and I. Wolff, "The near and far field distributions of a thin circular loop antenna in a radially multilayered biisotropic sphere," *Progress In Electromagnetics Research*, PIER 21, 103–135, 1999.

10. Li, W. C., M. S. Leong, P. N. Jiao, and W. X. Zhang, "Analysis of a passive circular loop antenna radiating in the presence of a layered chiral sphere using method of moments," *Journal of Electromagnetic Waves and Applications*, Vol. 16, No. 11, 1593–1611, 2002.

11. Li, L. W., M. S. Yeo, and M. S. Leong, "Method of moments analysis of EM fields in a multilayered spheroid radiated by a thin circular loop antenna," *IEEE Trans. Antennas Propag.*, Vol. 52, No. 9, 2391–2402, 2004.

12. Erma, V. A., "Exact solution for the scattering of electromagnetic waves from conductors of arbitrary shape. II. General case," *Physical Review*, Vol. 176, No. 5, 1544–1553, 1968.

13. Abramowitz, M. and I. A. Stegun, *Handbook of Mathematical Functions*, 437–438, National Bureau of Standards, Washington D.C., 1970.

14. Stratton, J. A., *Electromagnetic Theory*, 392–393, McGraw-Hill, New York, 1941.

15. Tai, C. T., *Dyadic Green Functions in Electromagnetic Theory*, 55–58, 48, 66, IEEE Press, New York, 1994.

16. Coxeter, H. S. and S. L. Greitzer, *Geometry Revisited*, 82–85, Mathematical Association of America, Washington D.C., 1967.

17. Balanis, C. A., *Antenna Theory*, 217–224, John Wiley & Sons, New York, 1997.